Catalysis Science & Technology

Emerging Investigators Series
Large Changes in Hydricity as a Function of Charge and Not Metal in (PNP)M-H (De)hydrogenation Catalysts That Undergo Metal-Ligand Cooperativity

Journal:	*Catalysis Science & Technology*
Manuscript ID	CY-ART-07-2022-001349.R2
Article Type:	Paper
Date Submitted by the Author:	20-Jan-2023
Complete List of Authors:	Schlenker, Kevin; University of Utah, Department of Chemistry Casselman, Lillee; University of Utah, Department of Chemistry Vanderlinden, Ryan; University of Utah, Department of Chemistry Saouma, Caroline; University of Utah, Department of Chemistry

SCHOLARONE™
Manuscripts

ARTICLE

Large Changes in Hydricity as a Function of Charge and Not Metal in (PNP)M-H (De)hydrogenation Catalysts That Undergo Metal-Ligand Cooperativity

Received 00th January 20xx,
Accepted 00th January 20xx

DOI: 10.1039/x0xx00000x

Kevin Schlenker,[a] Lillee K. Casselman,[a] Ryan T. VanderLinden,[a] Caroline T. Saouma*,[a]

Pincer-ligated catalysts that can undergo metal-ligand cooperativity (MLC), whereby H_2 is heterolytically cleaved (with proton transfer to the ligand and hydride transfer to the metal), have emerged as potent catalysts for the hydrogenation of CO_2 and organic carbonyls. Despite the plethora of systems developed that differ in metal/ligand identity, no studies establish how variation of the metal impacts the pertinent thermochemical properties of the catalyst, namely the equilibrium with H_2, the hydricity of the resulting hydride, and the acidity of the ligand. These parameters can impact the kinetics, scope, and mechanism of catalysis and hence should be established. Herein, we describe how changing the metal (Co, Fe, Mn, Ru) and charge (neutral vs. anionic) impacts these parameters in a series of PNP-ligated catalysts (PNP = 2,6-bis[(di-tert-butylphosphino)methyl]pyridine). A linear correlation between hydricity and ligand pK_a (when bound to the metal) is found, indicating that the two parameters are not independent of one another. This trend holds across four metals, two charges, and two different types of ligand (amine/amide and aromatization/dearomatization). Moreover, the effect of ligand deprotonation on the hydricity of **(PNP)(CO)(H)Fe-H** and **(PNP)(CO)(H)Ru-H** is assessed. It is determined that deprotonation to give anionic hydride species enhances the hydricity by ~ 16.5 kcal·mol^{-1} across three metals. Taken together, this work suggests that the metal identity has little effect on the thermodynamic parameters for PNP-ligated systems that undergo MLC via (de)aromatization, whilst the effect of charge is significant; moreover, ion-pairing allows for further tuning of the hydricity values. The ramifications of these findings for catalysis are discussed.

[a] *Department of Chemistry, University of Utah, Salt Lake City, Utah, 84112, U.S.A.*
Electronic Supplementary Information (ESI) available: Experimental details for the synthesis, characterization, thermochemical analysis (PDF) and crystallographic data (CCDC 2081604 and 2192117). See DOI: 10.1039/x0xx00000x

ARTICLE

Introduction

Metal hydrides (M-H) are implicated in many reactions that are pertinent to future energy schemes,[1] which include: photo- and electro-catalytic H_2 production,[2] combined carbon capture & recycling of CO_2,[3-5] bio-oil stabilization,[6] and use of liquid organic hydrogen carriers.[7, 8] Many of these processes are challenging because they necessitate the reduction of weakly electrophilic carbonyl species. Moreover, certain applications require that both the hydrogenation and dehydrogenation reactions occur under similar conditions. Given the role of M-H in these and other (de)hydrogenation reactions, it is important to understand how catalyst modification impacts their reactivity.

For catalysts that transfer net H_2, three thermodynamic parameters are critical to understanding the reactivity of the catalyst (Scheme 1, top): 1) the equilibrium of the catalyst with H_2 that generates a dihydride (or H_2 adduct; purple arrow), 2) the pK_a of the dihydride that gives a monohydride upon deprotonation (red arrow), and 3) the hydricity of the resulting monohydride (blue arrow). As shown in the bottom of Scheme 1, the same three parameters are pertinent for catalysts that undergo metal-ligand cooperativity (MLC). Now, the equilibrium with H_2 generates a monohydride with concomitant ligand protonation (purple arrow), and the protonated ligand pK_a is pertinent (red arrows) as is the hydride hydricity (blue arrows). Scheme 1 also shows how distinct mechanisms can deliver H_2 to a substrate via concerted H^+/H^- transfer (middle) or stepwise proton and hydride transfers (left, right) in MLC catalysts. Given the breadth of metal and ligand combinations in MLC catalysts,[9, 10] as well as the importance of these systems in advancing (de)hydrogenation reactions, establishing how the ligand and metal impact the thermodynamic parameters (Scheme 1, bottom) is timely. Thermodynamic understanding can provide insight to catalyst kinetics, mechanism, and scope, paving a route for rational catalyst design.

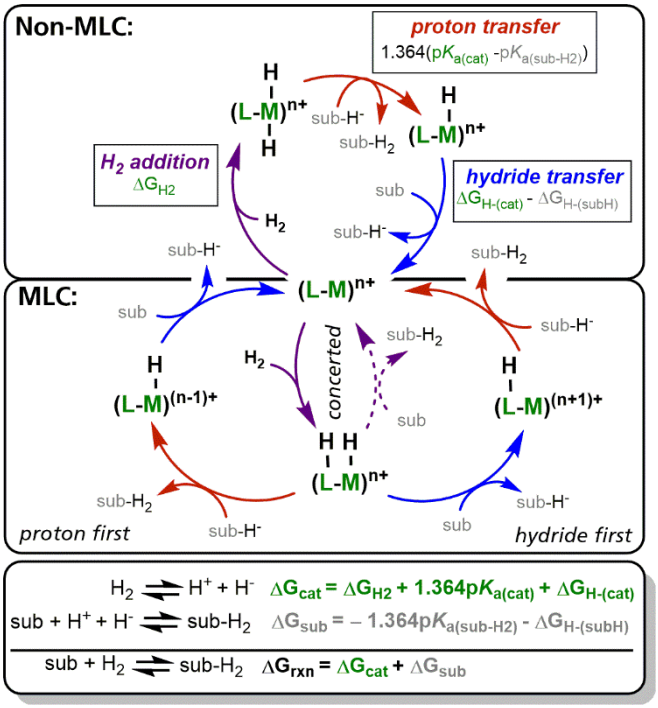

Scheme 1. Mechanism of H_2 transfer to a substrate at catalysts that do not undergo metal-ligand cooperativity (MLC) **(top)** and those that are capable of undergoing MLC **(middle)**. Catalysis that undergoes MLC can occur via sequential proton-hydride transfer (left), sequential hydride-proton transfer (right), or concerted transfer (middle, dashed). For simplicity, no substrate binding to the catalyst is shown, nor are mechanisms that involve solvent. The proton transfer step may occur with an external base, for example, in the hydrogenation of CO_2 to formate. **(bottom):** The overall free energy is comprised of catalyst and substrate contributions. The thermodynamics of each step should be matched to minimize energetic losses. ΔG_{cat} is equal to the energy to heterolytically cleave H_2 and hence is a constant that is solvent-dependent; the individual components in the equation (ΔG_{H2}, ΔG_{pKa}, and ΔG_{H-}) are unique to each catalyst. For clarity, the contributions to the overall reaction free energy are shown for the non-MLC mechanism.

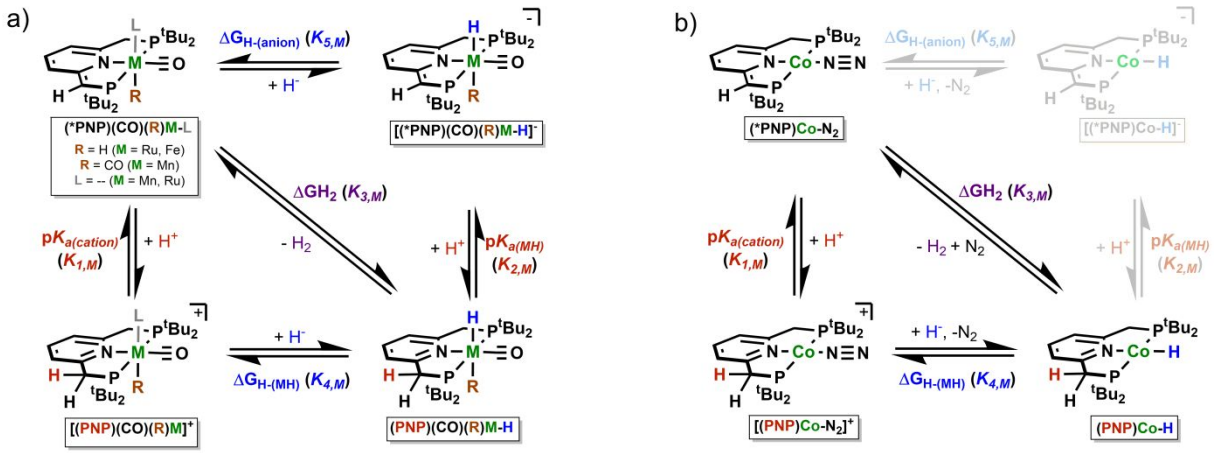

Scheme 2. a) Thermochemical parameters measured for Mn, Fe, and Ru. Only 5-coordinate Fe complexes bind a 6th neutral ligand, see text for details. L = -- indicates that L corresponds to a vacant coordination site. **b)** Thermochemical parameters measured for Co. The anionic hydride could not be generated, so its structure and associated thermodynamic parameters are greyed out. For clarity in naming, only the ligand that changes in the equilibria is placed after the metal.

Both experimental[11-17] and theoretical[18-20] studies suggest that kinetics can correlate with thermodynamics in hydrogenation reactions. The relationship is illustrated in the catalytic reduction of CO_2 to formate at phosphine ligated Co and Rh hydrides.[16] In this system, the Co-H are weakly hydridic (e.g., large values of ΔG_{H^-}), allowing for a linear relationship between the hydricity and log(TOF) to be observed (i.e., hydride transfer is rate-limiting). Conversely, the analogous Rh-H species that are very hydridic (e.g., small values of ΔG_{H^-}) show a linear relationship between the equilibrium with H_2 and log(TOF), as this step is now rate-limiting. In other instances, the correlation also suggests novel mechanisms.[13, 20] Hence, to increase overall kinetics, it is important to minimize free energy changes in the rate-determining step (Scheme 1).

Mechanistic insight can also be gleaned from an understanding of the catalyst and substrate thermodynamics (Scheme 1). For example, recent studies suggest that initial deprotonation of the ligand yields a more hydridic anionic metal hydride that is responsible for hydride transfer (Scheme 1, left).[21-24] This represents a new mechanistic hypothesis; yet anionic hydrides (that result from ligand deprotonation) remain under-explored in the literature. Related, an understanding of the thermodynamic parameters may indicate how the reaction conditions can alter the mechanism.[25-27] This knowledge could expand the types of reactions feasible with a single catalyst.[28]

Regarding scope, as shown in Scheme 1, the thermodynamics of the catalyst must match that of the substrate to avoid energetically prohibitive steps, which can also impact the overall kinetics (*vide supra*). This is illustrated in work by DuBois and coworkers; knowledge of how changing the catalyst impacts the thermodynamic parameters allowed for the development of electrocatalysts that either favor proton reduction or H_2 evolution.[29] Yang and coworkers recently extended this to catalysts that can both oxidize formate and reduce CO_2 near the thermodynamic potential.[30]

Despite the importance of investigating the thermodynamic parameters of catalysts, very few systems explore the parameters at hydrogenation catalysts that undergo MLC.[24, 28, 31] Throughout this manuscript, MLC represents catalysts in which the reaction with net H_2 results in electronic structure changes at the metal (i.e., a ligand formally alternates between being an L-type and LX-type donor),[32] not those in which ligand protonation is decoupled from hydride formation.[29] This motif has allowed for the development of catalysts that hydrogenate weakly electrophilic carbonyl substrates,[33, 34] and the replacement of Ru with 1st-row transition metals (Mn, Fe, Co).[10, 33-37] To establish how the metal identity impacts reactivity, it is important to consider the thermodynamic parameters described.[35]

Herein we describe the thermodynamic parameters of PNP-ligated neutral (Fe, Co) and anionic (Fe, Ru) hydrides and compare them to previously reported Mn[24] and Ru[28] analogues. In these systems, deprotonation occurs at a methylene proton, resulting in loss of aromatization in the central pyridine ring. This is the first study that establishes how changing the metal at MLC catalysts impacts the thermodynamic parameters. The ramifications of these findings for catalysis are discussed.

Results and discussion

Catalysts investigated and characterization of complexes.

The thermochemistry of four PNP-ligated M-H systems is considered (PNP = 2,6-bis[(di-tert-butylphosphino)methyl]pyridine; *PNP = deprotonated PNP; see Scheme 2 for structures). These hydrides are all invoked as intermediates for (de)hydrogenation reactions. Dihydrides **(PNP)(CO)(H)Fe-H**[38, 39] and **(PNP)(CO)(H)Ru-H**[9] are isoelectronic d^6

and 18-electron species. These are related to the manganese hydride, **(PNP)(CO)$_2$Mn-H**,[40-42] in which a hydride is replaced by a carbonyl to maintain charge and electron-count balance. Finally, the formally 16-electron and d^8 hydride, **(PNP)Co-H**[43-45] is also investigated.

Net transfer of H_2 from **(PNP)(CO)(R)M-H** to a substrate yields the de-aromatized species, **(*PNP)(CO)(R)M** (R = CO, M = Mn; R = H, M = Fe, Ru; see Scheme 2b for Co analogue) and hydrogenated substrate. Mechanistically, this could occur through the three routes shown in Scheme 1. The pertinent metal thermodynamic parameters and how they relate to one another for these mechanisms are shown in Scheme 2.

Prior to measuring the thermodynamic values shown in Scheme 2, all species must be characterized and shown to be stable on the time scale of measurements. With the exception of the anionic hydrides, **[Li][(*PNP)(CO)(H)M-H] (M = Fe, Ru)** and **(*PNP)(CO)(H)Fe**, the species shown in Scheme 2 are all reported in the literature.[24, 28, 39, 45-48] We have further characterized **[(PNP)(CO)(H)Fe]$^+$** in THF, which coordinates N_2 at reduced temperatures to give **[(PNP)(CO)(H)Fe-N$_2$]$^+$** (see ESI, section 2D). Room temperature data suggests that **[(PNP)(CO)(H)Fe]$^+$** is in equilibrium with **[(PNP)(CO)(H)Fe-L]$^+$**, where L is a terminal N_2 or THF.

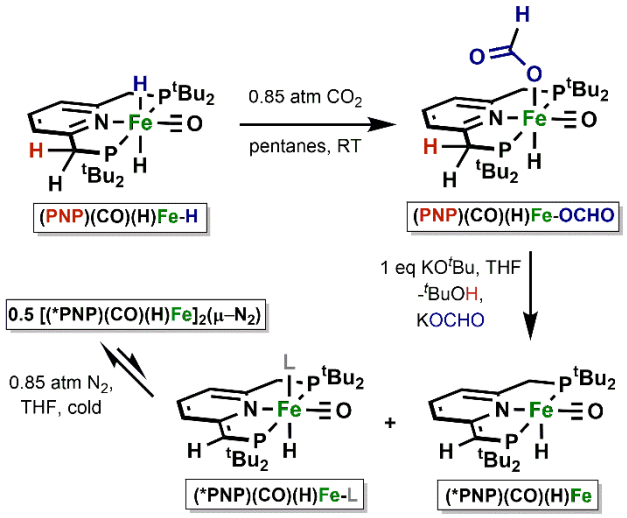

Scheme 3. Synthesis and equilibrium of **(*PNP)(CO)(H)Fe**. See ESI for details of the equilibrium speciation.

The synthesis of **(*PNP)(CO)(H)Fe** is accomplished following the procedure shown in Scheme 3. Briefly, **(PNP)(CO)(H)Fe-H** is first exposed to excess CO_2 to give the formate complex, **(PNP)(CO)(H)Fe-OCHO**. This species is then treated with one equivalent of KO^{t}Bu to give **(*PNP)(CO)(H)Fe** (along with loss of KOCHO and ^{t}BuOH). This approach is required because the steric bulk of the ^{t}Bu phosphine substituents precludes the synthesis of **(PNP)(CO)(H)Fe-Cl**, which can be directly deprotonated with the ^{i}Pr analogue.[49]

NMR characterization of **(*PNP)(CO)(H)Fe** is consistent with the proposed structures, whereby **(*PNP)(CO)(H)Fe** is in equilibrium at room temperature with **(*PNP)(CO)(H)Fe-L** (L = N_2 or THF, see ESI, section 2B). VT NMR and UV-vis data suggests that at reduced temperatures, **{(*PNP)(CO)(H)Fe}$_2$(μ-N$_2$)** (Scheme 3 and ESI) also forms. This equilibrium mixture of species is more stable than its ^{iPr}PNP counterpart,[49] though THF solutions still decompose to give free ligand, **(PNP)Fe(H)$_2$(CO)**, **(PNP)Fe(CO)$_2$**, and unidentified paramagnetic species over the course of 24 hours (see ESI). Owing to this degradation, equilibrium measurements were recorded upon mixing, and monitored over time to ensure that equilibrium was obtained in the absence of degradation (see ESI for details).

Anionic hydrides **[(*PNP)(CO)(H)M-H]$^-$ (M = Fe, Ru)** are readily prepared by addition of 1 equiv of ^{n}BuLi to **(PNP)(CO)(H)M-H**, akin to how **[Li][(*PNP)(CO)$_2$Mn-H]** is prepared.[24] The lithium cation can be exchanged to a potassium by addition of 1 equiv of KO^{t}Bu in the synthesis (Figure 1). Addition of a weak acid cleanly regenerates the neutral species (see Figures S19, S24), confirming that the observed reaction corresponds to a deprotonation. The anionic hydrides have been characterized by NMR spectroscopy. Notably, both of the ^{31}P NMR resonances shift upon encapsulation of the alkali metal cation in a crown-ether, suggesting that ion-pairing occurs in THF (see ESI).

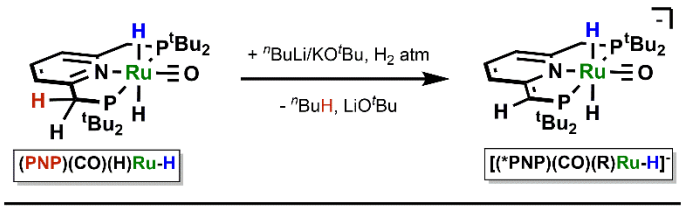

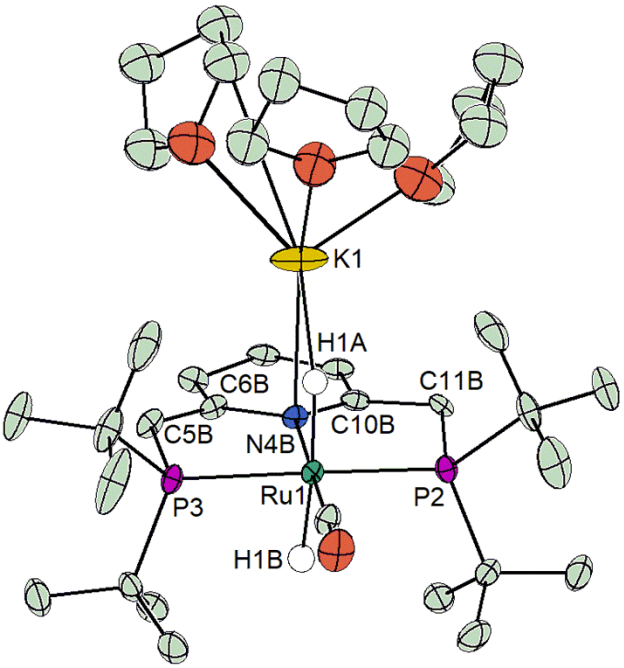

This journal is © The Royal Society of Chemistry 20xx

Please do not adjust margins

Figure 1. (top): Synthetic scheme to prepare **[K][(*PNP)(CO)(H)Ru-H]. (bottom):** Thermal ellipsoid plot of **[K][(*PNP)(CO)(H)Ru-H].** For clarity, all H-atoms that were not located in the difference map are omitted. The structure is disordered over which methylene is deprotonated (adjacent to P2 or P3), and only the major contribution is shown (56%). The disorder precludes accurate assessment of the C5B-C6B and C10B-C11B bond distances. Select bond distances (Å): N4B-K1: 2.85(2); C6B-K1: 3.22(2); C10B-K1: 3.22(2); Ru1-K1: 3.594(8). The minor component of the disorder has similar bond distances.

To further establish the ion-pairing, a crystal structure of **[K][(*PNP)(CO)(H)Ru-H]** was obtained (Figure 1). The potassium cation sits directly above the nitrogen and is equi-distant from both C6B and C10B. Disorder of the methyne/methylene position precludes accurate assessment of the bond distances; use of distance restraints were needed to give the best refinement. Both the ^{31}P and ^{1}H NMR data clearly suggest deprotonation of a single methylene position. Combined, this suggests the resonance structure shown in Figure 1, whereby deprotonation places an extra lone-pair on the nitrogen.

This is a rare example of what may be referred to as a formally 20-electron complex that arises from MLC.[28] However, the similar Ru-N bond distances in both the aromatized and dearomatized 6-coordinate species[28, 50, 51] suggest that the additional lone-pair on the nitrogen may not engage in bonding with the Ru. By contrast, the Ru-N distance in $N(CH_2CH_2P^{iPr}{}_2)_2Ru(CO)(H)$ is ~ 0.2 Å shorter than that in $HN(CH_2CH_2P^{iPr}{}_2)_2Ru(CO)(H)_2$,[52] suggesting that upon deprotonation of the amine to give an amide, the extra lone-pair does engage in bonding to the metal. Thus, **[K][(*PNP)(CO)(H)Ru-H]** is best referred to as an 18-electron species with a localized lone-pair on the nitrogen.

Ligand pK_a as a function of metal and charge.

To determine the pK_as of the various metal complexes (Scheme 2, p$K_{1,M}$ and p$K_{2,M}$), titrations of the protonated ligand congeners and suitable bases were conducted in THF and monitored by ^{31}P NMR spectroscopy (eq 1, see section 3 of the ESI for details). These deprotonation events occur at the methylene position of the ligand, and do not correspond to deprotonation of the metal hydride. The values obtained are summarized in Table 1. Attempts to deprotonate **(PNP)Co-H** did not give clean conversion to a new species, and hence it is not included in the analysis below.

Table 1. Measured pK_a (pK_{ip}) and extrapolated pK_α values.

Species[a]	pK_{ip}[b]	pK_α[c]	ΔpK_{ip} (p$K_{2,M}$- p$K_{1,M}$)
[(PNP)(CO)(H)Fe]$^+$	19.8[f]	19.7	13.0
(PNP)(CO)(H)Fe-H	32.8[g]	35.0	
[(PNP)(CO)(H)Ru]$^+$	20.7[d,h]	20.5	10.7
(PNP)(CO)(H)Ru-H	31.4[g]	33.6	
[(PNP)(CO)$_2$Mn]$^+$	18.8[e,f,h]	18.9[f] (18.6)[h]	12.4
(PNP)(CO)$_2$Mn-H	31.2[e,i]	32.5	
[(PNP)Co-N$_2$]$^+$	20.4[f]	20.3	--

[a]Deprotonation occurs on the ligand. [b]Error is ± 0.2 and calculated by propagation of uncertainty. [c]Error is ± 0.9 and calculated by propagation of uncertainty and multiplying by three. This is to emphasize that the errors in K_D are not known. [d]From ref [28]. [e]From ref [24]. [f]Counter-anion is $[BAr^F{}_4]^-$. [g]Counter-cation is [Ph(Me)C(H)-P(2,4,6-(MeO)$_3$-C$_6$H$_2$)$_3$]$^+$ [h]Counter-anion is $[BF_4]^-$. [i]Counter-cation is $[(Me_2)C(H)\text{-}PPh_3]^+$.

pK_{ip} versus pK_α. The values derived from the observed equilibria (eq 1) of the titrations correspond to the pK_{ip} (ip = ion-paired) of cationic species.[53, 54] These interactions are also sometimes called homoassociations.

$$[(\mathrm{HPNP})\mathrm{M}][\mathrm{A}] + \mathrm{B} \overset{K_D^{MA}}{\rightleftharpoons} [(\mathrm{HPNP})\mathrm{M}]^+ + [\mathrm{A}]^- + \mathrm{B} \overset{K_\alpha}{\rightleftharpoons} ({}^*\mathrm{PNP})\mathrm{M} + [\mathrm{A}]^- + [\mathrm{BH}]^+ \overset{(K_D^{BA})^{-1}}{\rightleftharpoons} ({}^*\mathrm{PNP})\mathrm{M} + [\mathrm{BH}][\mathrm{A}] \quad (1)$$

Unless explicitly noted, this is generally true for all pK_as reported in THF. This encompasses the true pK_a (termed pK_α) with two ion-pairing terms. The discrepancy between the two can be minimized by using similarly sized ions in the titrations such that the ion-pairing terms cancel. Alternatively, use of the Fuoss equation[55] allows for estimation of the ion-pairing term and determination of pK_α (more details can be found in the ESI). The similarly-sized ions used in the titrations give rise to small discrepancies (0.1 – 0.2) in the pK_{ip} and the pK_α values for the cationic acids of Table 1.

Deprotonation of the neutral metal hydrides with neutral bases involve a single ion-pair (eq 2). Hence, larger differences (1.3-1.5) in the pK_{ip} and the pK_α values are observed because ion-pairing effects do not negate one another.

$$[(\mathrm{HPNP})\mathrm{M}] + \mathrm{B} \overset{K_\alpha}{\rightleftharpoons} [({}^*\mathrm{PNP})\mathrm{M}]^- + [\mathrm{BH}]^+ \overset{(K_D)^{-1}}{\rightleftharpoons} [\mathrm{BH}][({}^*\mathrm{PNP})\mathrm{M}] \quad (2)$$

Unless noted, reference to pK_a in the text that follows refers to the pK_{ip}. As the pK_{ip}s were directly measured and the pK_αs estimated, throughout this manuscript, thermochemical parameters that are derived from the pK_a are reported using the pK_{ip}, with that derived from the pK_α immediately following in parentheses. Values derived with pK_α should be regarded as approximations, given that K_D in eqs 1 and 2 are approximations.

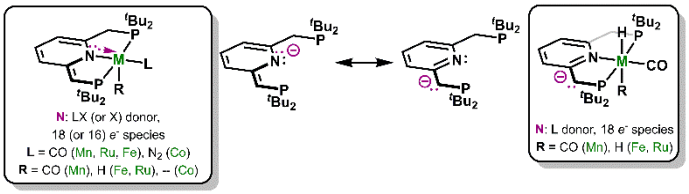

Figure 2. Resonance structures of the deprotonated (neutral) species.

pK_a values and trends. The observed deprotonations all occur at the ligand methylene position, though the lone-pair is delocalized onto the nitrogen through resonance (Figure 2). The cationic species span ~ 1.9 pK_a units (18.8-20.7), and are all lower than that of the free ligand (28.6).[28] The pK_a increases upon moving across the periodic table (Mn < Fe < Co ≤ Ru), though caution should be taken in over-interpreting this trend given the errors reported in Table 1. These values are all lower than that of the free ligand (28.6).[28] The decrease in pK_a of the ligand upon complexation with metal can be attributed to electrostatic effects: the cationic metal fragments are better at stabilizing the negative charge generated upon deprotonation (overall giving a neutral species). That the Mn species is the most acidic is consistent with it having two π-accepting carbonyl ligands (as opposed to one), allowing the negative charge to be further delocalized.

The pK_as of the neutral M-H species span 1.6 pK_a units (31.2-32.8) and appears to increase as Mn ≤ Ru < Fe. Going from cationic to neutral increases the pK_a by 10.7-13.0 pK_a units. Morris has derived an empirical formula to predict the pK_a of metal hydrides and dihydrogen adducts in THF (see ESI).[54] In the equation, going from a neutral to anionic conjugate base is predicted to increase the basicity by 30 pK_a units. While the equation does not hold for predicting the pK_a of the ligands in our system (see ESI), the increased basicity measured for the neutral M-H species (as opposed to cationic M fragments) is consistent with pK_a trends for metal hydride/dihydrogen adducts.

Taken together, the pK_as measured indicate that for the PNP ligand investigated, which may be representative of ligands that undergo aromatization/dearomatization, the metal fragment (comprised of the central metal and all non-PNP ligands) has little effect on the pK_a. For the Ru, Fe, and Mn species which are all isolobal, what impacts the pK_a the most is the addition of a negative charge, which also increases the formal electron count of the metal center from 18 to 20 in the deprotonated state.

Equilibrium of de-aromatized complexes with H_2 to yield M-H complexes.

The equilibrium of **(*PNP)(CO)(H)Fe** with partial pressures of H_2 to give **(PNP)(CO)(H)Fe-H** (Scheme 2, $K_{3,M}$) was monitored by UV-vis spectroscopy. From this, a value for $\Delta G_{H2,Fe}$ was found to be -3.8 ± 0.3 kcal·mol^{-1}. This value is similar to that obtained for the analogous Mn[24] and Ru[28] complexes (Table 2).

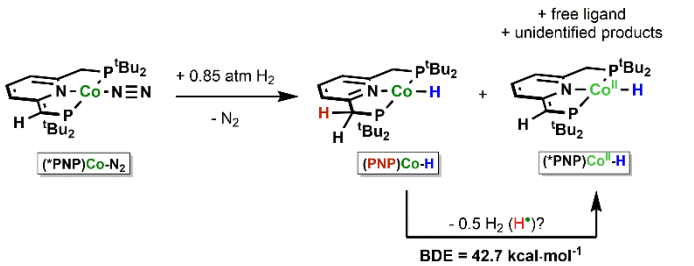

Scheme 4. Reactivity of **(PNP)Co-H**. BDE from ref [45]. BDE refers to the H-atom that is lost, which is the sum of methylene proton (red) loss and oxidation Co(I) to Co(II).

Addition of 0.85 atm of H_2 to **(*PNP)Co-N_2** gives a mixture of the desired **(PNP)Co^{I}-H** along with free ligand, **(*PNP)Co^{II}-H**, and other unidentifiable products (Scheme 4). Chirik and coworkers have also observed this reactivity, albeit at elevated temperatures.[45] It is conceivable that **(PNP)Co^{I}-H** is unstable to H-atom loss (with the proton coming from the methylene spacer and electron from the Co), generating **(*PNP)Co^{II}-H** and 0.5 equiv H_2. Indeed, the bond dissociation energy (BDE) of **(PNP)Co^{I}-H** was calculated to be 42.7 kcal·mol^{-1},[45] hence consistent with the release of 0.5 equiv of H_2 from **(PNP)Co^{I}-H**.

Direct measurement of $K_{3,Co}$ (Scheme 2b) is thus precluded by the lack of a clean equilibrium mixture. However, the equilibrium constant $K_{3,Co}$ and associated free energy can be determined from the pK_a and hydricity (*vide infra*); $\Delta G_{H2,Co}$ is found to be -2.3 ± 0.7 kcal·mol^{-1}.

Hydricity as a function of metal, charge, and formate binding.

Hydricity values were obtained by one of two methods.[1] The first makes use of the thermochemical cycle that combines the ligand acidity, the equilibrium with H_2, and the heterolysis of H_2 (Scheme 2). This approach allowed for determination of the hydricity values of **(PNP)(CO)(H)Fe-H** (eqs 4-7) and the two anionic hydrides, **[(*PNP)(CO)(H)M-H]**$^{-}$ (M = Ru, Fe; see *K*s of eqs 4-7).

$$(\mathbf{PNP})(\mathbf{CO})(\mathbf{H})\mathbf{Fe}-\mathbf{H} \rightleftarrows (^{*}\mathbf{PNP})(\mathbf{CO})(\mathbf{H})\mathbf{Fe}+\mathrm{H_2} \quad -\Delta G_{H2,M} \quad (K_{3,M})^{-1} \quad (4)$$

$$\mathrm{H_2} \rightleftarrows \mathrm{H^+ + H^-}\ [56] \quad \Delta G_{H2,het} = 68.7\ \mathrm{kcal\cdot mol^{-1}} \quad K_{H2,het} \quad (5)$$

$$(^{*}\mathbf{PNP})(\mathbf{CO})(\mathbf{H})\mathbf{Fe} + \mathrm{H^+} \rightleftarrows [(\mathbf{PNP})(\mathbf{CO})(\mathbf{H})\mathbf{Fe}]^{+} \quad -\Delta G_{H+,M} \quad (K_{1(or3),M})^{-1} \quad (6)$$

$$(\mathbf{PNP})(\mathbf{CO})(\mathbf{H})\mathbf{Fe}-\mathbf{H} \rightleftarrows [(\mathbf{PNP})(\mathbf{CO})(\mathbf{H})\mathbf{Fe}]^{+} + \mathrm{H^-} \quad \Delta G_{H-,M} \quad K_{4(or5),M} \quad (7)$$

The second approach considers the hydride transfer equilibrium with a hydride donor of known hydricity. Because the equilibrium that corresponds to eq 4 could not be experimentally determined for the Co system, the equilibrium of Figure 3 was probed in both directions. To ensure no loss of H_2 from **(PNP)(CO)(H)Ru-H**, the equilibrium was probed under an atmosphere of H_2 (none of the species in the equilibrium react with H_2). Though the Co species were too broad to accurately integrate, the absence of unidentifiable resonances, along with the same hydricity value being obtained in when both directions

This journal is © The Royal Society of Chemistry 20xx

Please do not adjust margins

of the equilibrium were probed ensures that the mass balance assumptions hold.

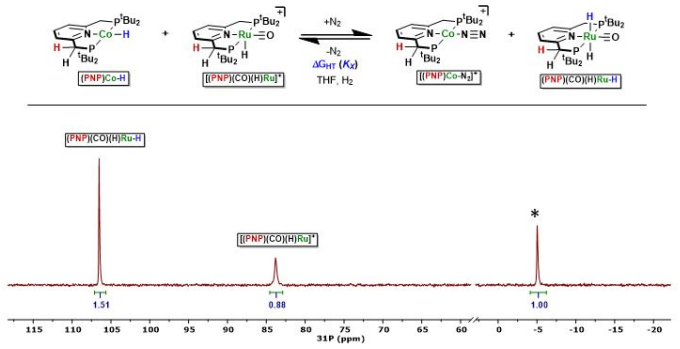

Figure 3. $^{31}P\{^1H\}$ NMR spectrum of the hydride transfer equilibrium between 1 equiv of **[(PNP)(CO)(H)Ru][BAr$_4^F$]** and 1 equiv of **(PNP)Co-H** in THF. K_X was determined from the integrations of the Ru species relative to the internal standard (*), triphenyl phosphate. From the integration, 63% of the Ru is **(PNP)(CO)(H)Ru-H** whilst only 37% remains as **[(PNP)(CO)(H)Ru][BAr$_4^F$]**.

Effect of metal. The hydricity values are summarized in Table 2. Values derived from pK_{ip}, which correspond to an ion-paired hydricity (i.e., [cation][M-H] → M + H$^-$ + cation), are reported with error. These are followed by approximations for the non-ion-paired hydricities (derived from pK_α), which are given in parentheses (i.e., [M-H]$^-$ → M + H$^-$).

The neutral Fe-H is less hydridic than the corresponding Ru-H by ~ 1 kcal·mol^{-1}. For the anionic hydrides, anionic Fe-H is more hydridic than the anionic Ru-H by ~ 2 kcal·mol^{-1}. Caution must be taken in over-interpreting these values given the errors reported in Table 2. Moreover, the neutral and anionic Fe-H hydricities may best be described as effective hydricities (*vide infra*), whereby an L-type ligand coordinates after hydride transfer, which does not occur in the Ru analogues. This L-type coordination enhances the hydricity, so the iron hydricity values should be taken as lower limits (i.e., the true hydricity value is larger). We note that periodic trends in hydricity[57-59] would suggest that the Ru should be significantly more hydridic than Fe. For example, phosphine-ligated metal hydrides of the Ni triad show that Pt and Pd counterparts are ~ 12 kcal·mol^{-1} more hydridic than the corresponding Ni hydrides.[57] Therefore, the similar hydricities observed for the Ru and Fe hydrides may be consistent with the trend if true hydricity was accessible; the subsequent binding of an L-type ligand to the Fe system precludes any quantitative comparisons.

Table 2. Hydricity values for **(PNP)(L)M-H** and **[(*PNP)(L)M-H]**$^-$ in THF.

M	ΔG_{H2}[a,b]	$\Delta G_{H-(neutral)}$[b]	$\Delta G_{H-(anion)}$[b]	$\Delta\Delta G_{H-}$	Effective $\Delta G_{H-}(OCHO)_{neutral}$[b]
Ru	-4.1 ± 0.2[c]	44.6 ± 0.6[c] (~44.8)	30.0 ± 0.3 (~27.0)	-14.7 (-16.9)	40.9 ± 0.9[c]
Fe	-3.8 ± 0.3	45.5 ± 0.4 (~45.6)	27.7 ± 0.4 (~24.8)	-17.8 (-19.9)	--
Mn	-3.3 ± 0.2[d]	46.4 ± 0.4[d] (~46.4)	29.5 ± 0.3[d] (~27.7)	-16.9[d] (-18.7)	~39.5[d]
Co	-2.7 ± 0.6[e]	43.6 ± 0.5 (~43.8)	--	--	36.7 ± 1.0

[a]Under standard state conditions of 1 atm. [b]Units of kcal·mol^{-1}. Errors obtained by propagation of error. Values in parentheses are obtained by using pK_α. No error is given as these are approximate values, given the uncertainty in K_D. [c]Reference [28]. [d]Reference [24]. [e]Extrapolated from eqs 4-7.

The neutral Mn-H appears to be less hydridic than the Fe-H by ~ 1 kcal·mol^{-1}. These complexes are both neutral 18-electron d^6 species (a hydride ligand on Fe is converted to a carbonyl on Mn). For pairs of iso-electronic metal hydrides that are next to one another on the periodic table, enhanced hydricity is observed by moving to the left. For example, comparing cationic Ni[60] to neutral Co[58] (and cationic Pd[57] to neutral Rh[61] indicates that the species on the left is ~ 14 kcal·mol^{-1} more hydridic. Both the magnitude and relative hydricity differs from the what we measured between Mn and Fe. However, this is not a direct comparison, as the iso-electronic pairs described above differ in charge, whilst the comparisons in the PNP system feature two neutral complexes. As in the neutral counterparts, anionic Mn-H is less hydridic than anionic Fe-H (by ~ 2 kcal·mol^{-1}), though caution must be taken to not over-interpret the results given the errors in Table 2. Taken together, this suggests that the metal identity may be less important than electrostatic effects when comparing iso-electronic hydrides that are next to one another on the periodic table (*vide infra*).[1]

The Co species appears to be the most hydridic of the neutral PNP-ligated metal hydrides. However, a direct comparison is misleading because **(PNP)Co-H** is a d^8, square planar species, and **(PNP)(CO)(R)M-H** are d^6, octahedral species (R = CO, Mn; R = H, Fe or Ru). Moreover, whereas the hydricity values for **(PNP)(CO)(R)M-H** correspond to true hydricities, the measured hydricity of **(PNP)Co-H** corresponds to an effective hydricity, as N_2 coordination follows hydride transfer (Scheme 5). The effective hydricity, which encompasses the hydricity with ligand coordination, has been shown to be smaller (more hydridic) than true hydricities because ligand binding is favourable (*vide infra*).[28, 62]

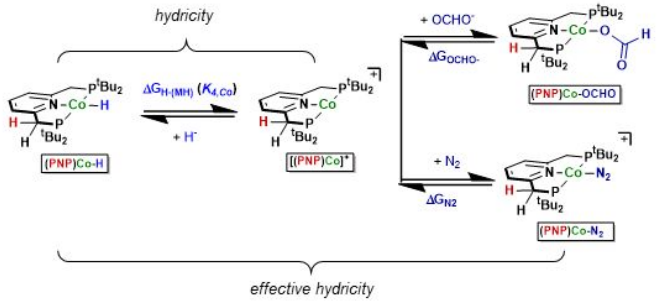

Scheme 5. Difference between hydricity and effective hydricity. Effective hydricity takes into account ligand binding such as N_2 or formate. See section 4G of the ESI for details regarding formate binding energy.

Effect of formate binding. To more directly compare the hydricity of the Co hydride with that of the other metals, the effective hydricity with formate binding was considered (Scheme 5). Given our interest in hydrogenating CO_2 to formate or MeOH, we sought to use formate as a pertinent ligand to compare effective hydricities with. Combining the hydricity and formate binding energy gives an effective hydricity of formate binding to Co of 36.7 kcal·mol^{-1}. This is more hydridic than the effective hydricity at Ru (40.9) and Mn (~ 39.5) upon formate binding. From the difference of the hydricity and effective hydricity values given in Table 2, we note that formate binding is almost twice as large for the Mn and Co complexes when compared to the Ru. The elimination of CO_2 from **(PNP)(CO)(H)Fe-OCHO** in THF[47] precludes the measurement of the effective hydricity at iron (see section 4B of the ESI).

Effect of charge. Deprotonation of **(PNP)(CO)(R)M-H (**R = CO, Mn; R = H, Fe or Ru) results in anionic hydrides that are ~ 16.5 (18.5) kcal·mol^{-1} more hydridic than their neutral counterparts (Table 2). This enhancement is observed with three metals, and hence may be general to the ligand and not the metal. Note, the difference in hydricity upon deprotonation is equal to the difference in free energy upon deprotonation (Hess' law; see Scheme 2 squares).

The enhanced hydricity may be rationalized by changes in the electron-count about the metal. If deprotonation results in a resonance structure whereby the electrons are localized on the nitrogen (Figure 2), as is observed in the solid-state structure of **[(*PNP)(CO)(H)Ru-H]**$^-$ (Figure 1), then hydride transfer gives the 5-coordinate 18-electron species **(*PNP)(CO)(H)Ru** (Scheme 2a). This should be more favorable than hydride transfer from **(PNP)(CO)(H)Ru-H** which gives the 5-coordinate 16-electron species **[(PNP)(CO)(H)Ru]**$^+$.

Conversely, the enhanced hydricity may be due to electrostatic interactions. If the deprotonation gives a localized pair of electrons on the ligand, then the neutral and anionic species are iso-electronic and simply differ by charge. The same is true if the electrons are localized on the nitrogen but not donating to the metal. The magnitude of the hydride enhancement upon gaining a negative charge is similar to that observed in comparing cationic and neutral iso-electronic metal species (lateral move on the periodic table, *vide supra*),[57, 58, 60, 61] suggesting that the enhanced hydricity observed in both series is primarily due to electrostatic effects.

The change in hydricity upon deprotonation is significant. For example, measured ground-state hydricities of stable transition metal hydrides in MeCN span ~ 51 kcal·mol^{-1}.[1] Thus, ligand deprotonation has the effect of spanning ~ a third the range, suggesting a new design element to tune hydricity without changing the metal. Also, when ion-pairing is taken into account (using pK_α in eq 6), the hydricity values of the anionic hydrides decrease by ~ 2 kcal·mol^{-1}. This suggests another mechanism to tune hydricity values in THF: by changing the size of the counterion, the ion-pairing contribution to acidity (and hence hydricity) can be modulated.

Interplay of Hydricity and Acidity

Towards the advancement of rational catalyst design, there is interest in establishing trends that allow for straightforward prediction of thermodynamic parameters such as hydricity,[57, 63] pK_a,[63, 64] and bond dissociation free energies[65] of metal hydrides.

A plot of hydricity versus pK_{ip} for all metal complexes for which these two parameters are known in THF is shown in Figure 4. A linear trend is observed, suggesting that the hydricity and pK_a are correlated. The slope of -1.322 is close to the predicted slope of -1.364 (from plotting eq 7 versus the pK_{ip}), and the intercept is the sum of 68.7 (free energy associated with H_2 heterolysis; eq 5)[56] and ΔG_{H2}. This indicates that all complexes have similar ΔG_{H2} in THF. Hence, the pK_{ip} and hydricity values counter-balance one another and cannot be independently tuned. The plot of hydricity versus pK_a gives a similar slope and intercept (see Figure S56).

This analysis shows that as the metal identity and charge of PNP-ligated metal hydrides is varied, a correlation between the hydricity and ligand pK_a is observed. The thermodynamic parameters of both **(al-^{iPr}PNP)(CO)(H)Fe-H**[31] and **(al-^{Cy}PNP)(CO)(H)Ru-H**,[66] catalysts that can undergo MLC (Figure 4, bottom), also fits the line. This is significant because now deprotonation occurs at a metal-bound amine to give an amide. While there appears to be a trend, caution should be taken in using pK_a to directly estimate hydricity in complexes that can undergo MLC until this approach can be validated with more complexes. We simply note that the hydricity and ligand pK_a are not independent of one another.

This journal is © The Royal Society of Chemistry 20xx

Please do not adjust margins

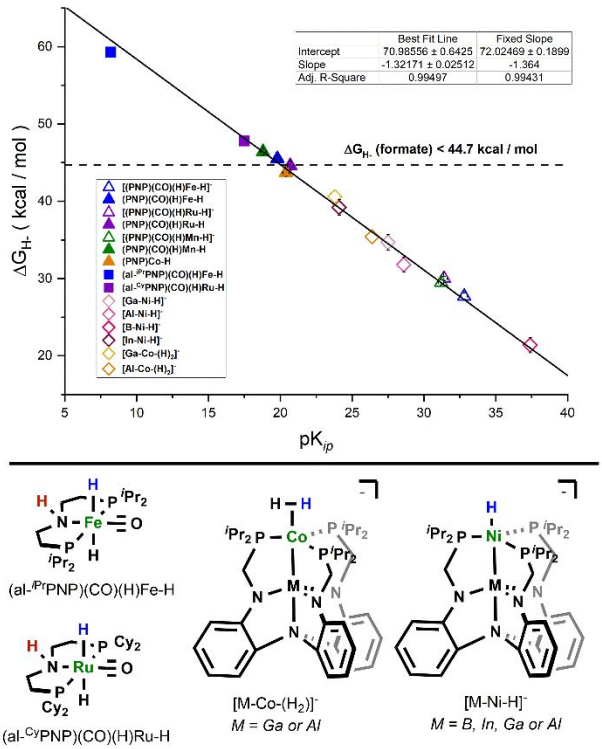

Figure 4. (top): Plot of hydricity versus pK_a in for all known complexes in THF. Hydricity values in ref [17] reported relative to H_2 and hence were converted by adding 68.7 kcal·mol^{-1}.[56] Black line corresponds to the fixed slope equation. **(bottom):** Structures of other metal hydrides for which the thermochemical parameters are known in THF; the hydride for which the hydricity corresponds to is shown in blue. The site of deprotonation is shown in red for other systems that undergo MLC. For [M-Co-(H_2)]$^-$, the pK_{ip} refers to deprotonation of the hydride of M-Co-H(H_2).[17] For [M-Ni-H]$^-$, the pK_{ip} refers to deprotonation the coordinated dihydrogen of M-Ni-(H_2).[67]

The plot of Figure 4 also includes two M-Co and four M-Ni complexes for which pertinent thermodynamic data is available.[17, 67] These do not undergo MLC, and their fit to the line may be coincidental, or suggest that in THF, hydricity is generally correlated with acidity. We emphasize that more data is required before conclusions can be made regarding broad trends across types of complexes or temperature.

The results shown in Figure 4 contrasts the thermodynamic tuning achieved at P_2N_2-ligated Ni complexes (see ESI).[68-73] In this system, hydride transfer occurs at the metal while proton transfer occurs at the pendant amine ligand (a second pendent amine can deprotonate the M-H, resulting in an oxidation-state change). However, unlike the systems studied in this work, ligand protonation occurs with no change in the metal electronic structure (i.e., one ligand formally going from L to LX). Variation of the phosphine substituents (while keeping the amine substituents constant) allows for tuning of the hydricity whilst keeping the pK_a constant (and hence shifting the equilibrium with H_2). Conversely, variation of the amine substituents (while keeping the phosphine substituents constant) changes the pK_a whilst maintaining a constant hydricity (and again shifting the equilibrium with H_2). Plots are shown in section 4I of the ESI. Hence, the hydricity and pK_a are completely decoupled at P_2N_2-ligated Ni, which can represent a different type of MLC.

Ramifications for Catalysis

Understanding the thermodynamic parameters associated with net transfer of H_2 is pertinent to understanding mechanisms and advancing catalyst design principles. The parameters reported in this work allow for several conclusions to be drawn.

First, deprotonation of the ligand results in enhancement of the hydricity by ~ 16.5 (18.5) kcal·mol^{-1} (Table 2). The enhancement appears primarily to be an electrostatic effect, and hence suggests a new ligand design strategy for grossly changing the hydricity: changing the overall charge of the ligand or using a ligand that can be deprotonated under basic conditions.[74] Our work is the first to show how charge (without changing any other parameters) impacts hydricity. When charge is modulated by changing the metal oxidation-state at a Ru complex, a similar-sized change in hydricity is observed; modulating the ligand oxidation-state in that system results in a smaller change in hydricity.[75] By contrast, recent work from the Yang group suggests that charge has minimal impact on metal hydride bond dissociation free energies.[76]

With regards to catalysis, we have shown that **(PNP)(CO)$_2$Mn-H** serves as a precatalyst for the hydrogenation of CO_2 to formate, and that formate production ensues from an anionic hydride.[24] Given that CO_2 hydrogenation to formate requires stoichiometric base, it is conceivable that more broadly, anionic hydrides are mechanistically pertinent at catalysts that can undergo MLC. Catalysis that overall transfer a net H_2 equivalent and hence does not necessitate stoichiometric base may also proceed through anionic hydrides. For example, Bergens showed that deprotonation of Noyori-type Ru catalysts is required for hydrogenation of amides and imides at low temperature.[23] Szymczak showed that ligand deprotonation and coordination of an alkali metal cation impacts the electronics of a Ru-H complexes and enhances the rate of transfer hydrogenations;[77] in this system hydride transfer was shown to be rate-limiting, and the alkali-metal is proposed to help orient the ketone substrate. More recently, Kempe and co-workers showed that ketimines and aldimines can be hydrogenated by a di-deprotonated Mn complex with sub-stoichiometric base (relative to substrate).[21] Kinetic evidence supports the requirement for double deprotonation by KO^{t}Bu, with the proton transfer occurring from the resulting ^{t}BuOH. Given the generality of deprotonation described here (Mn, Ru, Fe), the magnitude in the hydricity change, and the plethora of hydrogenations that necessitate catalytic amounts of base,[10, 35, 36] anionic hydrides should be considered.

A direct comparison of hydricity values in THF and MeCN is not possible due to solvent effects that impact hydricity to differing extents.[78] As points of reference, the hydricity of H_2 is 76.0 kcal·mol^{-1} in MeCN and 68.7 kcal·mol^{-1} in THF,[56] yet the estimated hydricity of formate is similar in the two solvents (MeCN[63]: 44.0

kcal·mol^{-1}; THF[28]: 44.7 kcal·mol^{-1}). The hydricity of an anionic Re hydride was recently reported to be 3 kcal·mol^{-1} more hydridic in THF than MeCN,[14] and very recently, Lu and co-workers reported that [B-Ni-H]$^-$ has a hydricity of 21.4 kcal·mol^{-1} in THF.[67] With this caveat in mind, the anionic hydrides described here may be amongst the most hydridic ground-state metal hydrides that are sufficiently stable for characterization. In MeCN, the most hydridic 1st row metal hydride has a hydricity of 31.8 kcal·mol^{-1} (the most hydridic ground-state metal hydride has a hydricity of 26.6 kcal·mol^{-1}).[1]

In particular, the anionic hydride **[(PNP)(CO)(H)Fe-H]**$^-$ has a hydricity value of 24.8 kcal·mol^{-1} when no ion-pairing is assumed to occur. This is 2 kcal·mol^{-1} more hydridic than when ion-pairing is present, and suggests that the hydride may be rendered more anionic if a crown-ether can encapsulate the alkali cation, akin to how TMEDA renders alkyl lithium reagents more nucleophilic. Moreover, the ion-pair interaction should be tuneable by using different sized cations, which is the subject of ongoing studies in our group.

Second, changing the metal does not significantly impact the thermodynamic parameters at PNP-ligated metal centres whereby deprotonation results in de-aromatization. Consequently, in the absence of gross differences in mechanism, it is predicted that similar bases and H_2 pressures should yield similar results amongst these four catalysts under otherwise similar conditions. This contrasts with the larger changes in thermodynamic parameters observed upon changing the metal in systems that undergo MLC via amine deprotonation[31, 66] and systems that cannot undergo MLC[17] (*vide supra*). Moreover, in the P_2N_2 system, changing the metal from Ni to Rh greatly alters the thermodynamic parameters; the Rh[79] congeners are *ca*. 30 kcal·mol^{-1} more hydridic than the Ni[68, 70] analogues.

Taken together, this suggests that for catalysts capable of undergoing MLC via aromatization/dearomatization, both 1st and 2nd row transition metals should have similar thermodynamic limitations (and hence potentially scope). Indeed, Mn has emerged in recent years as being capable of doing much of the same chemistry as Ru.[10, 35, 36] We emphasize that this is strictly a thermodynamic argument, and does not take into account possible changes in kinetics or possible reaction pathways. For example, Co has been shown to undergo 1-electron chemistry,[45] which may alter the overall reactions feasible as well as introduce more mechanistic proposals.

Third, the plot of hydricity versus pK_a suggests that the two thermodynamic parameters may be correlated in systems that undergo MLC. This result warrants further studies to determine if this can be generalized more broadly for catalysts capable of undergoing MLC, for catalysts in THF, and to determine if the trend holds as a function of temperature. By contrast, independent tuning of the hydricity and pK_a can be achieved in the P_2N_2 system.

Finally, this work establishes the hydricities of metal hydrides at systems that can undergo MLC via aromatization/dearomatization. Figure 4 indicates that the neutral metal hydrides are near the hydricity of formate in THF and that the anionic congeners are significantly more hydridic. The hydricities of Co-M and Ni-M bimetallic hydrides (with exception of the Ni-B system),[17, 67] and that of an anionic Re species (37.6 kcal·mol^{-1})[14] lie between the two regions of the MLC catalysts. This re-enforces the effect that charge has on hydricity. This trend, with anionic hydrides being more reducing (smaller hydricity values) is qualitatively similar to the observation made by Kubiak and co-workers, whereby plots of hydricity versus the second reduction potential are linear.[63]

Many studies on catalysts that undergo MLC suggest either concerted transfer (Scheme 1, bottom middle) or sequential hydride-proton transfer (Scheme 1, bottom right).[9, 10, 80] If concerted transfer occurs with related catalysts, then similar substrate scopes for (de)hydrogenations are predicted (assuming no gross changes in mechanism or stability concerns). This is a consequence of our work that shows similar thermodynamics associated with H_2 addition across catalysts (Scheme 1, purple and Figure 4). While the acidity and equilibrium with H_2 may only be pertinent to mechanisms that invoke MLC, the hydricity value is broadly pertinent to hydrogenation catalysts, regardless of the mechanism. This work is thus relevant to the ongoing debate[81-83] in the role that MLC plays in catalytic mechanisms.

Conclusions

The pK_a, equilibrium with H_2, and hydricity were evaluated and compared for a series of PNP-ligated metal hydrides that differ in metal identity and charge. This is the first study that compares the thermochemical parameters of (de)hydrogenation catalysts that can undergo MLC. It was found that for all complexes, the equilibrium with H_2 remains ~ constant because the hydricity and pK_a counterbalance one another. While changing the metal identity impacts the hydricity and pK_a, these changes are small (for systems whereby deprotonation results in loss of aromaticity) compared to the effect that deprotonation has on these thermodynamic parameters. Given that many catalytic transformations are run under stoichiometric or catalytic quantities of base, deprotonated and anionic metal hydrides should be considered as plausible in proposed mechanistic schemes.

Author Contributions

K. S. carried out the experiments, analysed the experimental data and aided in conceptualization. R. T. V. collected and analysed the XRD data. L. K. C. made figures for the revised manuscript. C. T. S. conceptualized and supervised the work. K. S. and C. T. S. wrote the manuscript, with input from R. T. V. C. T. S. and L. K. C. revised the manuscript, with input from the other authors.

This journal is © The Royal Society of Chemistry 20xx

Please do not adjust margins

Conflicts of interest

There are no conflicts to declare.

Acknowledgements

The authors gratefully acknowledge start-up funding from the University of Utah & USTAR, and NSF CAREER (1945646). National Institutes of Health awards 1C06RR017539-01A1 and 3R01GM063540-17W1 are acknowledged for construction and maintenance of the NMR facilities. We thank Dr. Peter Flynn for help with NMR experiments, Eleni Spanolios for insightful discussions.

Notes and references

1. E. S. Wiedner, M. B. Chambers, C. L. Pitman, R. M. Bullock, A. J. M. Miller and A. M. Appel, *Chemical Reviews*, 2016, **116**, 8655-8692.
2. J. R. McKone, S. C. Marinescu, B. S. Brunschwig, J. R. Winkler and H. B. Gray, *Chemical Science*, 2014, **5**, 865-878.
3. W.-H. Wang, Y. Himeda, J. T. Muckerman, G. F. Manbeck and E. Fujita, *Chemical Reviews*, 2015, **115**, 12936-12973.
4. K. Sordakis, C. Tang, L. K. Vogt, H. Junge, P. J. Dyson, M. Beller and G. Laurenczy, *Chemical Reviews*, 2018, **118**, 372-433.
5. M. Bhattacharya, S. Sebghati, R. T. VanderLinden and C. T. Saouma, *Journal of the American Chemical Society*, 2020, **142**, 17589-17597.
6. C. H. Lam, W. Deng, L. Lang, X. Jin, X. Hu and Y. Wang, *Energy & Fuels*, 2020, **34**, 7915-7928.
7. P. Preuster, C. Papp and P. Wasserscheid, *Accounts of Chemical Research*, 2017, **50**, 74-85.
8. A. Kumar, T. Janes, N. A. Espinosa-Jalapa and D. Milstein, *Journal of the American Chemical Society*, 2018, **140**, 7453-7457.
9. C. Gunanathan and D. Milstein, *Chemical Reviews*, 2014, **114**, 12024-12087.
10. L. Alig, M. Fritz and S. Schneider, *Chemical Reviews*, 2019, **119**, 2681-2751.
11. J. E. Heimann, W. H. Bernskoetter, N. Hazari and James M. Mayer, *Chemical Science*, 2018, **9**, 6629-6638.
12. S. Ramakrishnan, K. M. Waldie, I. Warnke, A. G. De Crisci, V. S. Batista, R. M. Waymouth and C. E. D. Chidsey, *Inorganic Chemistry*, 2016, **55**, 1623-1632.
13. C. S. Seu, A. M. Appel, M. D. Doud, D. L. DuBois and C. P. Kubiak, *Energy & Environmental Science*, 2012, **5**, 6480-6490.
14. J. Hu, Q. J. Bruch and A. J. M. Miller, *Journal of the American Chemical Society*, 2021, **143**, 945-954.
15. J. D. Erickson, A. Z. Preston, J. C. Linehan and E. S. Wiedner, *ACS Catalysis*, 2020, **10**, 7419-7423.
16. M. S. Jeletic, E. B. Hulley, M. L. Helm, M. T. Mock, A. M. Appel, E. S. Wiedner and J. C. Linehan, *ACS Catalysis*, 2017, **7**, 6008-6017.
17. M. V. Vollmer, J. Ye, J. C. Linehan, B. J. Graziano, A. Preston, E. S. Wiedner and C. C. Lu, *ACS Catalysis*, 2020, **10**, 2459-2470.
18. B. Mondal, F. Neese and S. Ye, *Inorganic Chemistry*, 2015, **54**, 7192-7198.
19. B. Mondal, F. Neese and S. Ye, *Inorganic Chemistry*, 2016, **55**, 5438-5444.
20. L. Xue and M. S. G. Ahlquist, *Inorganic Chemistry*, 2014, **53**, 3281-3289.
21. F. Freitag, T. Irrgang and R. Kempe, *Journal of the American Chemical Society*, 2019, **141**, 11677-11685.
22. C. A. Huff and M. S. Sanford, *ACS Catalysis*, 2013, **3**, 2412-2416.
23. J. M. John, S. Takebayashi, N. Dabral, M. Miskolzie and S. H. Bergens, *Journal of the American Chemical Society*, 2013, **135**, 8578-8584.
24. K. Schlenker, E. Christensen, A. Zhanserkeev, G. McDonald, E. Yang, K. Lutz, R. Steele, R. VanderLinden and C. T. Saouma, *submitted.*, 2021.
25. T. Huang, E. S. Rountree, A. P. Traywick, M. Bayoumi and J. L. Dempsey, *Journal of the American Chemical Society*, 2018, **140**, 14655-14669.
26. J. J. Warren, T. A. Tronic and J. M. Mayer, *Chemical Reviews*, 2010, **110**, 6961-7001.
27. S. A. Burgess, A. M. Appel, J. C. Linehan and E. S. Wiedner, *Angewandte Chemie International Edition*, 2017, **56**, 15002-15005.
28. C. L. Mathis, J. Geary, Y. Ardon, M. S. Reese, M. A. Philliber, R. T. VanderLinden and C. T. Saouma, *Journal of the American Chemical Society*, 2019, **141**, 14317-14328.
29. D. L. DuBois, *Inorganic Chemistry*, 2014, **53**, 3935-3960.
30. D. W. Cunningham, J. M. Barlow, R. S. Velazquez and J. Y. Yang, *Angewandte Chemie International Edition*, 2020, **59**, 4443-4447.
31. J. B. Curley, N. E. Smith, W. H. Bernskoetter, M. Z. Ertem, N. Hazari, B. Q. Mercado, T. M. Townsend and X. Wang, *ACS Catalysis*, 2021, **11**, 10631-10646.
32. J. R. Khusnutdinova and D. Milstein, *Angewandte Chemie International Edition*, 2015, **54**, 12236-12273.
33. A. Kumar, T. Janes, N. A. Espinosa-Jalapa and D. Milstein, *Angewandte Chemie International Edition*, 2018, **57**, 12076-12080.
34. U. K. Das, A. Kumar, Y. Ben-David, M. A. Iron and D. Milstein, *Journal of the American Chemical Society*, 2019, **141**, 12962-12966.
35. T. Zell and R. Langer, *ChemCatChem*, 2018, **10**, 1930-1940.
36. G. A. Filonenko, R. van Putten, E. J. M. Hensen and E. A. Pidko, *Chemical Society Reviews*, 2018, **47**, 1459-1483.
37. N. Gorgas and K. Kirchner, *Accounts of Chemical Research*, 2018, **51**, 1558-1569.
38. J. A. Garg, S. Chakraborty, Y. Ben-David and D. Milstein, *Chemical Communications*, 2016, **52**, 5285-5288.
39. R. Langer, Y. Diskin-Posner, G. Leitus, L. J. W. Shimon, Y. Ben-David and D. Milstein, *Angewandte Chemie International Edition*, 2011, **50**, 9948-9952.
40. Y.-Q. Zou, S. Chakraborty, A. Nerush, D. Oren, Y. Diskin-Posner, Y. Ben-David and D. Milstein, *ACS Catalysis*, 2018, **8**, 8014-8019.
41. J. Masdemont, J. A. Luque-Urrutia, M. Gimferrer, D. Milstein and A. Poater, *ACS Catalysis*, 2019, **9**, 1662-1669.

This journal is © The Royal Society of Chemistry 20xx

Please do not adjust margins

42. A. Mukherjee and D. Milstein, *ACS Catalysis*, 2018, **8**, 11435-11469.
43. E. Khaskin, Y. Diskin-Posner, L. Weiner, G. Leitus and D. Milstein, *Chemical Communications*, 2013, **49**, 2771-2773.
44. M. L. Scheuermann, S. P. Semproni, I. Pappas and P. J. Chirik, *Inorganic Chemistry*, 2014, **53**, 9463-9465.
45. S. P. Semproni, C. Milsmann and P. J. Chirik, *Journal of the American Chemical Society*, 2014, **136**, 9211-9224.
46. S. M. Rummelt, H. Zhong, N. G. Léonard, S. P. Semproni and P. J. Chirik, *Organometallics*, 2019, **38**, 1081-1090.
47. T. Zell, B. Butschke, Y. Ben-David and D. Milstein, *Chemistry – A European Journal*, 2013, **19**, 8068-8072.
48. E. Khaskin, M. A. Iron, L. J. W. Shimon, J. Zhang and D. Milstein, *Journal of the American Chemical Society*, 2010, **132**, 8542-8543.
49. R. Langer, G. Leitus, Y. Ben-David and D. Milstein, *Angewandte Chemie International Edition*, 2011, **50**, 2120-2124.
50. J. Zhang, G. Leitus, Y. Ben-David and D. Milstein, *Angewandte Chemie International Edition*, 2006, **45**, 1113-1115.
51. E. R. M. Habraken, A. R. Jupp, M. B. Brands, M. Nieger, A. W. Ehlers and J. C. Slootweg, *European Journal of Inorganic Chemistry*, 2019, **2019**, 2436-2442.
52. E. Alberico, A. J. J. Lennox, L. K. Vogt, H. Jiao, W. Baumann, H.-J. Drexler, M. Nielsen, A. Spannenberg, M. P. Checinski, H. Junge and M. Beller, *Journal of the American Chemical Society*, 2016, **138**, 14890-14904.
53. J. Saame, T. Rodima, S. Tshepelevitsh, A. Kütt, I. Kaljurand, T. Haljasorg, I. A. Koppel and I. Leito, *The Journal of Organic Chemistry*, 2016, **81**, 7349-7361.
54. K. Abdur-Rashid, T. P. Fong, B. Greaves, D. G. Gusev, J. G. Hinman, S. E. Landau, A. J. Lough and R. H. Morris, *Journal of the American Chemical Society*, 2000, **122**, 9155-9171.
55. R. M. Fuoss, *Journal of the American Chemical Society*, 1958, **80**, 5059-5061.
56. K. R. Brereton, C. N. Jadrich, B. M. Stratakes and A. J. M. Miller, *Organometallics*, 2019, **38**, 3104-3110.
57. C. J. Curtis, A. Miedaner, J. W. Raebiger and D. L. DuBois, *Organometallics*, 2004, **23**, 511-516.
58. R. Ciancanelli, B. C. Noll, D. L. DuBois and M. R. DuBois, *Journal of the American Chemical Society*, 2002, **124**, 2984-2992.
59. A. D. Wilson, A. J. M. Miller, D. L. DuBois, J. A. Labinger and J. E. Bercaw, *Inorganic Chemistry*, 2010, **49**, 3918-3926.
60. D. E. Berning, B. C. Noll and D. L. DuBois, *Journal of the American Chemical Society*, 1999, **121**, 11432-11447.
61. J. W. Raebiger and D. L. DuBois, *Organometallics*, 2005, **24**, 110-118.
62. C. L. Pitman, K. R. Brereton and A. J. M. Miller, *Journal of the American Chemical Society*, 2016, **138**, 2252-2260.
63. K. M. Waldie, A. L. Ostericher, M. H. Reineke, A. F. Sasayama and C. P. Kubiak, *ACS Catalysis*, 2018, **8**, 1313-1324.
64. R. H. Morris, *Journal of the American Chemical Society*, 2014, **136**, 1948-1959.
65. B. E. Rennie, R. G. Eleftheriades and R. H. Morris, *Journal of the American Chemical Society*, 2020, **142**, 17607-17629.
66. C. L. Mathis, PhD, University of Utah, 2020.
67. J. R. Prat, R. C. Cammarota, B. J. Graziano, J. T. Moore and C. C. Lu, *Chemical Communications*, 2022, DOI: 10.1039/D2CC03219H.
68. B. R. Galan, J. Schöffel, J. C. Linehan, C. Seu, A. M. Appel, J. A. S. Roberts, M. L. Helm, U. J. Kilgore, J. Y. Yang, D. L. DuBois and C. P. Kubiak, *Journal of the American Chemical Society*, 2011, **133**, 12767-12779.
69. J. Y. Yang, S. E. Smith, T. Liu, W. G. Dougherty, W. A. Hoffert, W. S. Kassel, M. R. DuBois, D. L. DuBois and R. M. Bullock, *Journal of the American Chemical Society*, 2013, **135**, 9700-9712.
70. K. Fraze, A. D. Wilson, A. M. Appel, M. Rakowski DuBois and D. L. DuBois, *Organometallics*, 2007, **26**, 3918-3924.
71. U. J. Kilgore, M. P. Stewart, M. L. Helm, W. G. Dougherty, W. S. Kassel, M. R. DuBois, D. L. DuBois and R. M. Bullock, *Inorganic Chemistry*, 2011, **50**, 10908-10918.
72. S. Wiese, U. J. Kilgore, D. L. DuBois and R. M. Bullock, *ACS Catalysis*, 2012, **2**, 720-727.
73. A. Jain, S. Lense, J. C. Linehan, S. Raugei, H. Cho, D. L. DuBois and W. J. Shaw, *Inorganic Chemistry*, 2011, **50**, 4073-4085.
74. Y. M. Badiei, W.-H. Wang, J. F. Hull, D. J. Szalda, J. T. Muckerman, Y. Himeda and E. Fujita, *Inorganic Chemistry*, 2013, **52**, 12576-12586.
75. Y. Matsubara, E. Fujita, M. D. Doherty, J. T. Muckerman and C. Creutz, *Journal of the American Chemical Society*, 2012, **134**, 15743-15757.
76. A. D. Cypcar, T. A. Kerr and J. Y. Yang, *Organometallics*, 2022, **41**, 2605-2611.
77. C. M. Moore, B. Bark and N. K. Szymczak, *ACS Catalysis*, 2016, **6**, 1981-1990.
78. C. Tsay, B. N. Livesay, S. Ruelas and J. Y. Yang, *Journal of the American Chemical Society*, 2015, **137**, 14114-14121.
79. A. M. Lilio, M. H. Reineke, C. E. Moore, A. L. Rheingold, M. K. Takase and C. P. Kubiak, *Journal of the American Chemical Society*, 2015, **137**, 8251-8260.
80. H. Li and M. B. Hall, *ACS Catalysis*, 2015, **5**, 1895-1913.
81. L. N. Dawe, M. Karimzadeh-Younjali, Z. Dai, E. Khaskin and D. G. Gusev, *Journal of the American Chemical Society*, 2020, **142**, 19510-19522.
82. P. A. Dub, B. L. Scott and J. C. Gordon, *Journal of the American Chemical Society*, 2017, **139**, 1245-1260.
83. P. A. Dub and J. C. Gordon, *ACS Catalysis*, 2017, **7**, 6635-6655.

This journal is © The Royal Society of Chemistry 20xx

Please do not adjust margins